Numerical Heat Transfer, Part A: Applications: An International Journal of Computation and Methodology
Publication details, including instructions for authors and subscription information:
http://www.tandfonline.com/loi/unht20

AN ASSESSMENT OF k-ω AND v ^{2}-f TURBULENCE MODELS FOR STRONGLY HEATED INTERNAL GAS FLOWS

Robert E. Spall [a] , Adam Richards [a] & Donald M. McEligot [b]
[a] Department of Mechanical and Aerospace Engineering , Logan, Utah, USA
[b] Idaho National Engineering and Environmental Engineering Laboratory , Idaho Falls, Idaho, USA
Published online: 17 Aug 2010.

To cite this article: Robert E. Spall , Adam Richards & Donald M. McEligot (2004) AN ASSESSMENT OF k-ω AND v ^{2}-f TURBULENCE MODELS FOR STRONGLY HEATED INTERNAL GAS FLOWS, Numerical Heat Transfer, Part A: Applications: An International Journal of Computation and Methodology, 46:9, 831-849, DOI: 10.1080/104077890504032

To link to this article: http://dx.doi.org/10.1080/104077890504032

Numerical Heat Transfer, Part A, 46: 831–849, 2004

ISSN: 1040-7782 print/1521-0634 online
DOI: 10.1080/104077890504032

Taylor & Francis
Taylor & Francis Group

AN ASSESSMENT OF k–ω AND v^2–f TURBULENCE MODELS FOR STRONGLY HEATED INTERNAL GAS FLOWS

Robert E. Spall and Adam Richards
Department of Mechanical and Aerospace Engineering, Utah State University, Logan, Utah, USA

Donald M. McEligot
Idaho National Engineering and Environmental Engineering Laboratory, Idaho Falls, Idaho, USA

Both k–ω and v^2–f turbulence models are used to model an axisymmetric, strongly heated, low-Mach-number gas flowing upward within a vertical tube in which forced convection is dominant. The heating rates are sufficiently high, so that fluid properties vary significantly in both the axial and radial directions; consequently, fully developed mean flow profiles do not evolve. Comparisons between computational results and experimental results, which exist in the literature, reveal that the v^2–f model performs quite well in predicting axial wall temperatures, and mean velocity and temperature profiles. This may be contrasted with the k–ω model results, in which the wall heat transfer rates and near-wall velocities are significantly overpredicted.

INTRODUCTION

This work is concerned with the modeling of a strongly heated, low-Mach-number gas flowing upward within a vertical tube with (nearly) constant heat flux boundary conditions in which forced convection is dominant. The heating rate is sufficiently high, so that the fluid properties vary significantly in both the radial and axial directions. Since the flow is continually adjusting to the changing properties, fully developed velocity and temperature profiles never occur.

The motivation for this problem stems from considerations that gas may be effectively employed as a coolant for advanced power reactors. In this case, it is desirable to achieve high thermal efficiencies, which require high gas exit temperatures.

Received 5 March 2004; accepted 18 June 2004.

Robert Spall and Adam Richards acknowledge support from the Inland Northwest Research Alliance (INRA) to pursue this research. The participation of Prof. Donald M. McEligot was partially supported by the U.S.-RoK I-NERI program under DOE Idaho Field Office Contract DE-AC07-99ID13727.

Address correspondence to Robert E. Spall, Department of Mechanical and Aerospace Engineering, UMC 4130, Utah State University, Logan, UT 84322-4130, USA. E-mail: spall@engineering.usu.edu

NOMENCLATURE

C_p	specific heat	u_τ	friction velocity
D	tube diameter	U_i	Reynolds-averaged mean velocity component
f	elliptic relaxation function	$\overline{v^2}$	velocity variance scale
g	gravity	x_i	spatial coordinate
G	mean axial mass flux per unit area	y	wall normal distance
k	turbulence kinetic energy	y^+	dimensionless wall normal distance
L	length scale		
Nu	Nusselt number		
p	pressure	ε	dissipation rate
P	turbulence production	λ	thermal conductivity
Pr_t	turbulent Prandtl number	μ	dynamic viscosity
q	dimensional heating rate	μ_t	eddy viscosity
q^+	dimensionless heating rate	ν	kinematic viscosity
R	ideal gas constant	ρ	density
Re	Reynolds number	τ	turbulence time scale
T	temperature	ω	specific dissipation rate

To achieve high temperatures, the mean velocity of the gas may be low enough that the relevant Reynolds number of the flow is less than 10,000.

Experimental data for this class of flows is sparse. Perkins [1] obtained mean temperature distributions for dominant forced-convection flow through a circular cylinder with significant gas property variations. Using essentially the same experimental apparatus, Shehata [2] obtained mean velocity distributions under some of the same flow conditions. These authors employed three different constant wall heat flux boundary conditions: "low" and "intermediate" heating rates at inlet Reynolds numbers of approximately 6,000, and a "high" heating rate case at an inlet Reynolds number of approximately 4,200. Perkins [1] characterized these three cases as turbulent, "subturbulent," and laminarizing, respectively. The results of Perkins [1] and Shehata [2] have since been reported in detail by Shehata and McEligot [3, 4]. Consequently, subsequent references to the Shehata/McEligot data refer to the data as presented in [3] and [4], derived from the results of Perkins [1] and Shehata [2]. These experimental data provide an opportunity to verify turbulence models under the influence of strong heating and, consequently, large variations in fluid properties.

Of particular importance for accurate heat transfer predictions using turbulence models is the approach taken for the near-wall modeling. Methodologies include: (1) the use of wall functions, (2) zonal approaches, which use a simplified formulation in the near-wall region, (3) the use of damping functions, (4) change from dissipation rate, ε, to alternative variables that are well behaved in the viscous sublayer, and (5) elliptic relaxation.

Several computational fluid dynamics predictions of the Shehata/McEligot [3] experiments using damping functions and alternative variable formulations are available in the literature. In particular, Mikielewicz et al. [5] presented results for a k–τ model and a number of low-Reynolds-number k–ε models. Their general conclusion was that most of these models gave poor results, greatly underpredicting the wall-to-bulk fluid temperature difference. However, the k–ε model of Launder and Sharma [6] was deemed to provide reasonable results.

The $\mathrm{Re} = 4{,}300$ case presented by Shehata and McEligot [3, 4] resulted in near laminarization of the flow due to strong heating. From an application standpoint, this situation may be an undesirable development, since heat transfer parameters may be diminished and wall temperatures increased. Direct numerical simulations (DNS) of flow through a tube under these conditions were performed by Satake et al. [7]. Their DNS results, in terms of integral parameters, compared well with those from the experiments, approaching laminar values at downstream stations. Although difficult to measure experimentally, the DNS results also indicated that the high heating rates led to a significant reduction in the Reynolds shear stress, further indicating a laminarization of the initially turbulent flow.

Other "advanced" turbulence models have also been used to model the Shehata/McEligot experiments. For instance, Ezato et al. [8] extended the k–ε model of Abe et al. [9], originally developed for constant-property flows, to model the Shehata/McEligot experiment. Subsequently, Nishimura et al. [10] utilized a differential Reynolds stress transport model with turbulent heat flux and thermal energy fluctuation equations. Each of these approaches provided reasonable predictions of mean velocity and temperature distributions to model the same flow.

Additional related work includes that of Takase [11–13], who applied k–ε models to the flow through an annular fuel channel model, and annular models with ribs, for Reynolds numbers between 3,000 and 20,000. By adding correction terms and adjusting model constants, it appears that he was able to obtain results that one might consider adequate for engineering analyses. Fujii et al. [14] also conducted experimental and numerical investigations using two-equation eddy viscosity models for heat transfer of a strongly heated gas flow in an annular duct. At low heat fluxes, all models tested performed satisfactorily. However, the same was not true at the higher heat fluxes, with predicted heat transfer coefficients up to 20% below those found experimentally.

In this article, we investigate the performance of v^2–f and low-Reynolds-number k–ω models in predicting the Shehata/McEligot experiments. Advantageously, both of these models may be integrated through the viscous sublayer without the use of damping functions. However, low-Reynolds-number viscous corrections, which are commonly applied to the k–ω model, have been implemented in this work (c.f. [15]).

The v^2–f model, which is not as commonly used as other turbulence models, was developed from a simplified second-moment closure approach and involves the solution of three transport equations for the turbulence quantities k, ε, and $\overline{v^2}$, and an elliptic equation for near-wall and nonlocal effects [16]. The model extends the standard k–ε model by incorporating near-wall turbulence anisotropy, while retaining a linear eddy viscosity approximation. The $\overline{v^2}$ term is taken as the velocity scale for the evaluation of the turbulent viscosity; it is proportional to k far from the wall, but in the near-wall region, it represents the velocity fluctuation normal to the surface. The model has been successfully used to model heat transfer using constant-property assumptions for channel and impinging jet flows [17, 18]. Alternative formulations of the v^2–f model, which address deficiencies identified in the earlier models, have been developed. In particular, Manceau et al. [19] use an alternative scaling for the elliptic relaxation function to improve log-layer predictions, while others have utilized homogeneous boundary conditions on the elliptic function to

improve robustness [20, 21]. The model (and closure constants) described in [21] is utilized in the work presented herein.

Results obtained using k–ω and v^2–f models are first compared against a standard experimental correlation for constant-property flows available in the literature. The models are then used to predict integral and mean flow quantities under the high-heat-flux, variable-property conditions of the Shehata/McEligot experiments [3]. The performance of the two models in predicting these variable-property flows is assessed. We note that in performing these calculations, the values of the turbulence closure coefficients employed were those values given in the literature, and that no effort was made to tune the coefficients to improve predictions of the flows considered herein.

GOVERNING EQUATIONS

The Reynolds-averaged Navier-Stokes and energy equations, along with the v^2–f and k–ω closure models, are expressed in Cartesian tensor notation as follows. *Continuity equation:*

$$\frac{\partial}{\partial x_i}(\rho U_i) = 0 \tag{1}$$

Momentum equations:

$$\frac{\partial}{\partial x_j}(\rho U_j U_i) = -\frac{\partial \tilde{p}}{\partial x_i} + \frac{\partial}{\partial x_j}\left[(\mu + \mu_t)\left(\frac{\partial U_i}{\partial x_j} + \frac{\partial U_j}{\partial x_i}\right)\right] - \rho g_i \tag{2}$$

where, for purposes of numerical implementation, we have defined a modified pressure as

$$\tilde{p} = p + \frac{2}{3}(\mu + \mu_t)\frac{\partial U_j}{\partial x_j} + \frac{2}{3}\rho k \tag{3}$$

Energy equation:

$$\frac{\partial}{\partial x_j}(\rho C_p U_j T) = \frac{\partial}{\partial x_j}\left[(\lambda + \lambda_t)\frac{\partial T}{\partial x}\right] \tag{4}$$

where the effective thermal conductivity, λ_t, is defined as

$$\lambda_t = \frac{C_p \mu_t}{Pr_t}. \tag{5}$$

The k–ε–v^2–f Turbulence Model Equations

The equations for k and ε for the v^2–f model are written as

$$\frac{\partial}{\partial x_i}(\rho U_i k) = P - \rho\varepsilon + \frac{\partial}{\partial x_j}\left[\left(\mu + \frac{\mu_t}{\sigma_k}\right)\frac{\partial k}{\partial x_j}\right] \tag{6}$$

$$\frac{\partial}{\partial x_i}(\rho U_i \varepsilon) = \frac{C^*_{\varepsilon 1} P - C_{\varepsilon 2}\rho\varepsilon}{\tau} + \frac{\partial}{\partial x_j}\left[\left(\mu + \frac{\mu_t}{\sigma_\varepsilon}\right)\frac{\partial \varepsilon}{\partial x_j}\right] \tag{7}$$

where

$$P = 2\mu_t S^2 \qquad S^2 = S_{ij}S_{ij} \qquad S_{ij} = \frac{1}{2}\left(\frac{\partial U_i}{\partial x_j} + \frac{\partial U_j}{\partial x_i}\right)$$

The turbulent viscosity, μ_t, is given by the relation

$$\mu_t = \rho C_\mu \overline{v^2} \tau \tag{8}$$

where τ is a turbulent time scale, given as

$$\tau^* = \max\left(\frac{k}{\varepsilon}, 6\sqrt{\frac{\nu}{\varepsilon}}\right) \tag{9}$$

$$\tau = \min\left(\tau^*, \frac{\chi}{\sqrt{3}}\frac{k}{\overline{v^2} C_\mu \sqrt{2S^2}}\right) \tag{10}$$

The governing equations for $\overline{v^2}$ and f are

$$\frac{\partial}{\partial x_i}(\rho U_i \overline{v^2}) = \rho k f - 6\rho \overline{v^2}\frac{\varepsilon}{k} + \frac{\partial}{\partial x_j}\left[\left(\mu + \frac{\mu_t}{\sigma_k}\right)\frac{\partial \overline{v^2}}{\partial x_j}\right] \tag{11}$$

$$f - L^2 \frac{\partial^2 f}{\partial x_j \partial x_j} = (C_1 - 1)\frac{(2/3 - \overline{v^2}/k)}{\tau} + C_2 \frac{P}{\rho k} + \frac{5\overline{v^2}/k}{\tau} \tag{12}$$

The length scale, L, appearing in the elliptic relaxation equation for f is given as

$$L^* = \min\left(\frac{k^{3/2}}{\varepsilon}, \frac{1}{\sqrt{3}}\frac{k^{3/2}}{\overline{v^2} C_\mu \sqrt{2S^2}}\right) \tag{13}$$

$$L = C_L \max\left[L^*, C_\eta\left(\frac{\nu^3}{\varepsilon}\right)^{1/4}\right] \tag{14}$$

The closure coefficients for the model, as published in [21], are given as $\chi = 0.6$, $C_1 = 1.4$, $C_2 = 0.3$, $C_{\varepsilon 1} = 1.4$, $C_{\varepsilon 2} = 1.9$, $C_\eta = 70$, $C_\mu = 0.22$, $C_L = 0.23$, $\sigma_k = 1.0$, $\sigma_\varepsilon = 1.3$, and $C^*_{\varepsilon 1} = C_{\varepsilon 1}\left(1 + 0.045\sqrt{k/\overline{v^2}}\right)$. We note that no effort was made to recalibrate these coefficients to improve flow predictions.

The wall boundary conditions for the k and ε equations are given as $k = 0$ and $\varepsilon = (2\nu k_1)/y_1^2$. For the v^2–f equations, the boundary conditions are $\overline{v^2} = 0$ and $f = 0$. The subscript 1 indicates that values are taken as those at the center of the computational cell adjacent to the wall.

The Low-Reynolds-Number k–ω Turbulence Model Equations

$$\frac{\partial}{\partial x_i}(\rho U_i k) = P - \rho\beta^* k\omega + \frac{\partial}{\partial x_j}\left[\left(\mu + \frac{\mu_t}{\sigma_k}\right)\frac{\partial k}{\partial x_j}\right] \tag{15}$$

$$\frac{\partial}{\partial x_i}(\rho U_i \omega) = \frac{\alpha\omega}{k}P - \rho\beta\omega^2 + \frac{\partial}{\partial x_j}\left[\left(\mu + \frac{\mu_t}{\sigma_\omega}\right)\frac{\partial \omega}{\partial x_j}\right] \tag{16}$$

The turbulent viscosity is determine from the relation

$$\mu_t = \frac{\alpha^* \rho k}{\omega} \tag{17}$$

The coefficients α, α^*, and β^* defined below provide low-Reynolds-number damping corrections.

$$\alpha = \frac{\alpha_\infty}{\alpha^*}\left(\frac{\alpha_0 + \mathrm{Re}_t/\mathrm{Re}_\omega}{1 + \mathrm{Re}_t/\mathrm{Re}_\omega}\right) \tag{18}$$

$$\alpha^* = \alpha_\infty^*\left(\frac{\alpha_0^* + \mathrm{Re}_t/\mathrm{Re}_k}{1 + \mathrm{Re}_t/\mathrm{Re}_k}\right) \tag{19}$$

$$\beta^* = \beta_\infty^*\left[\frac{4/15 + (\mathrm{Re}_t/\mathrm{Re}_\beta)^4}{1 + (\mathrm{Re}_t/\mathrm{Re}_\beta)^4}\right] \tag{20}$$

$$\mathrm{Re}_t = \frac{\rho k}{\mu\omega} \tag{21}$$

The closure coefficients for the k–ω model are given as $\beta = 0.072$, $\beta_\infty^* = 0.09$, $\alpha_0^* = \beta/3$, $\alpha_\infty^* = 1.0$, $\alpha_\infty = 0.52$, $\alpha_0 = 1/9$, $R_k = 6$, $R_\omega = 2.95$, $R_\beta = 8$, $\sigma_k = 2.0$, and $\sigma_\omega = 2.0$ [15].

The boundary condition on ω is given as

$$\omega = \frac{2500\tau_w}{(k^+)^2\mu}$$

with k_s^+ set to unity, corresponding to a hydraulically smooth surface (where $k_s^+ = u_\tau k_s/\nu$ and k_s is the average height of sand-grain roughness elements) [15]. The boundary condition on k is given as $k = 0$.

NUMERICAL PROCEDURE

The governing equations were solved in an axisymmetric, cylindrical coordinate system using a pressure-based finite-volume formulation on a staggered grid [22]. Pressure–velocity coupling was accomplished using the SIMPLE algorithm. All viscous terms within the governing equations were discretized using second-order central differencing. Using deferred correction, a blended second-order central differencing was implemented for the convection terms. That is, fluxes at cell faces were determined as $F = F_L + (F_H - F_L)^{\text{old}}$, where F_H represents a second-order central differencing scheme, and F_L represents a first-order upwind scheme [23]. The blending factor, β, was set to 0.8 to eliminate oscillations that might occur in regions of high gradients when using a pure central difference scheme. The discretized v^2–f equations were solved in a coupled manner using a block-tridiagional solver. All other discretized equations were solved sequentially, using a point successive over-relaxation scheme.

The calculations were completed on a base-level grid consisting of 200 points in the streamwise direction and 101 points in the radial direction. For all cases, $y^+ < 0.5$ at the center of the control volume adjacent to the wall. In addition to clustering toward the wall, grid points were clustered near $x/D = 0$ to resolve the rapid variations in wall temperatures that occur in this region (due to the onset of the wall heat flux). Grid convergence was evaluated by solving the system on coarser 100×101 and 200×51 grids. A discussion of these results appears in the Results section.

The property variations for density and viscosity were defined by the incompressible ideal gas law and Sutherland's law, respectively. Polynomial fits were used to define the thermal conductivity and specific heat. In particular,

$$\rho = \frac{P_{\text{ref}}}{RT} \tag{22}$$

$$\mu = \mu_0 \left(\frac{T}{T_0}\right)^{1.5} \left(\frac{T_0 + S}{T + S}\right) \tag{23}$$

$$\lambda = 6.64465 \times 10^{-3} + 7.1845 \times 10^{-5} T - 1.3276 \times 10^{-8} T^2 \tag{24}$$

$$C_p = 1.0526 \times 10^{3} - 2.8029 \times 10^{-1} T + 4.2562 \times 10^{-4} T^2 \tag{25}$$

where $\mu_0 = 1.7894 \times 10^{-5}\,\text{N} \cdot \text{s/m}^2$, $T_0 = 273.11$, $S = 110.56$, and $p_{\text{ref}} = 92{,}400$ Pa. In addition, the turbulent Prandtl number used in the definition of the effective thermal conductivity was set to the constant value of 0.85 [24].

INLET AND WALL THERMAL BOUNDARY CONDITIONS

The test section described by Shehata and McEligot [3, 4] was constructed of resistively heated, seamless, extruded Inconel 600 tube of $D = 0.0274$ m inside

diameter. Their experimental apparatus was set up to provide axisymmetric, steady, fully developed turbulent flow at the start of the heating section. The origin of the heated tube section began at $x/D = 0$. However, axial conduction along the test section walls resulted in elevated wall temperatures for $\sim$15 tube diameters upstream of the origin. This conduction was handled in the numerical simulations by fixing the wall temperatures to the experimentally measured values for $x/D < 0$. In addition, end-wall effects also resulted in a drop in the heat flux near the end of the heated section.

Over the heated section, the wall thermal boundary conditions are consistent with those presented in Shehata and McEligot [3], in which dimensionless heating rates were defined as

$$q^+ = \frac{q_w}{GC_p T_{\text{in}}} \tag{26}$$

where q_w is the mean wall heat flux, T_{in} is the inlet temperature, and G is the mean axial mass flux per unit area. Following the notation in Shehata and McEligot [3], we designate three distinct cases as Run 618, Run 635, and Run 445. Run 618 represents a low-heating-rate turbulent case with $q^+ \approx 0.0018$ and an inlet Reynolds number (based on tube diameter, D) of approximately 6,000. Run 635 represents a "subturbulent," intermediate-heating-rate case with $q^+ \approx 0.0035$ and an inlet Reynolds number of approximately 6,000. Run 445 represents a "laminarizing," high-heating-rate case with $q^+ \approx 0.0045$ and an inlet Reynolds number of approximately 4,200. For the numerical calculations, curve-fits to the wall heat flux data presented in [3] were employed for the wall thermal boundary conditions (for $x/D = 0$).

The inlet of the computational domain was specified at $x/D = -15.615$, and the outlet at $x/D = 29$. Fully developed profiles were specified as the inlet boundary conditions. To be consistent, the inlet profiles used for each of the models were those resulting from fully developed flow solutions computed using each model, respectively. These profiles for mean velocity and turbulence kinetic energy are shown in Figures 1*a* and 1*b*, respectively. Experimental data for the mean velocity as provided in [3] are included in Figure 1*a*. However, experimental data were not available for the turbulence kinetic energy. Temperatures at the inlet to the computational domain, T_{in}, were set to uniform values between 296 and 297.7 K, depending on the experimentally measured data for each specific case.

RESULTS

We first present results for fully developed, constant wall heat flux, constant-property flows at Reynolds numbers of interest in this study. The motivation behind this is that models that cannot accurately predict these flows are unlikely to be able to predict the more complex variable-property flows inherent in the Shehata/McEligot experiments. Subsequently, we present results for the Shehata/McEligot cases previously denoted as Runs 618, 635, and 445, which correspond

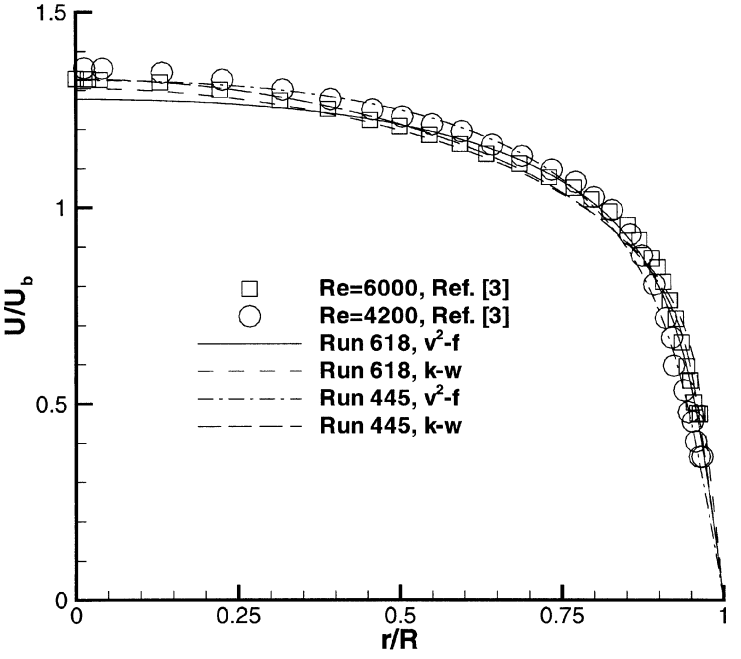

(*a*)

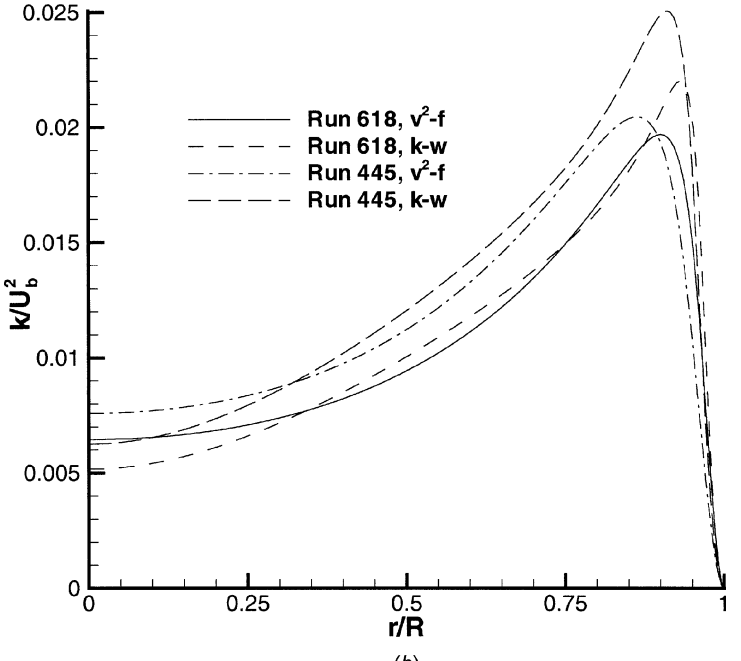

(*b*)

Figure 1. (*a*) Comparison between experimental [3] and computed fully developed inlet velocity profiles. (*b*) Fully developed inlet profiles of turbulence kinetic energy computed using v^2–f and k–ω turbulence models.

to increasing levels of dimensionless wall heat flux. Results presented include computed wall temperatures, and mean flow velocity and temperature profiles.

Constant-Property Flows

These calculations were performed to examine the performance of the turbulence models under conditions of constant wall heat flux and constant fluid properties. Under these conditions, the velocity and thermal fields are not coupled, and fully developed velocity and (nondimensional) temperature profiles can occur. Calculations were performed using both turbulence models over a range of Reynolds numbers below 10,000, with a Prandtl number of 0.72. Shown in Figure 2 are the computed Nusselt numbers as a function of Reynolds number. The Nusselt number results have been normalized with respect to the well-known Dittus/Boelter [25] correlation for fully developed turbulent flow in a tube, given as $\mathrm{Nu} = 0.021\,\mathrm{Re}^{0.8}\,\mathrm{Pr}^{0.4}$. Note that the correlation coefficient of 0.021 is slightly different than the original value of 0.023. McEligot et al. [26] indicate that a coefficient of 0.021 provides improved fits over the original value. The results reveal that the v^2–f model predicted the Nusselt number with reasonable accuracy over the Reynolds number range $3{,}000 \leq \mathrm{Re} \leq 10{,}000$ of interest in this study. However, there is a slight upward trend in the Nusselt number prediction as the Reynolds number is increased. In contrast, the k–ω model significantly overpredicted the Nusselt number, although the trend is toward the correlation results as the Reynolds number is increased. Consequently, the k–ω model should not be

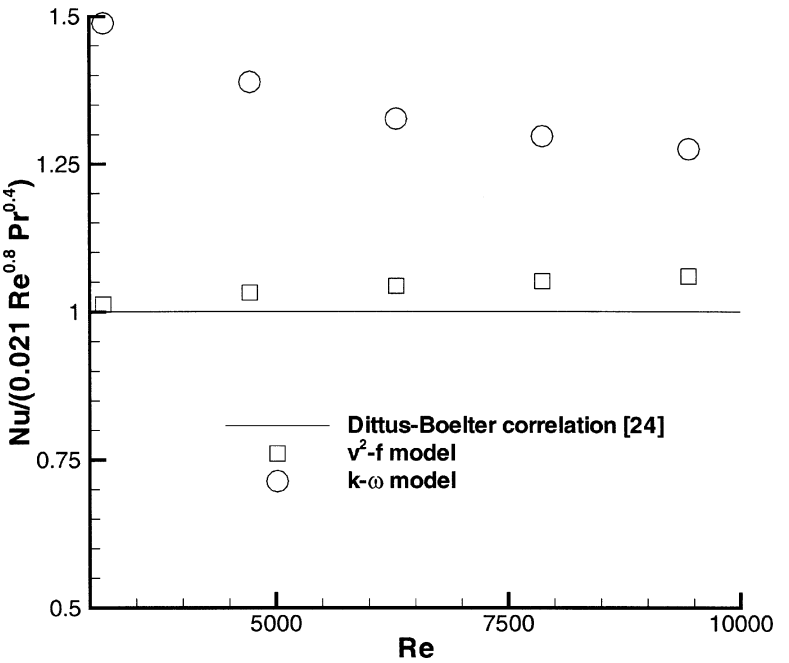

Figure 2. Low-Reynolds-number predictions for fully developed flow in a circular tube with constant fluid properties.

expected to perform well in predicting the more challenging variable-property flows at the low Reynolds numbers inherent in the Shehata/McEligot experiments. In particular, the overprediction of the Nusselt number for these flows with the constant-property assumption suggests that quantities, such as the tube wall temperature, will be underpredicted.

Variable-Property Flows

We present, in Figure 3, wall temperatures as a function of x/D for the three wall heat flux cases denoted as Runs 618, 635, and 445, where x/D is measured from the start of the heated section. As stated previously, the inlet flow profiles were obtained from computational solutions for fully developed isothermal flow at the measured mass flow rate for each case. The results are consistent with what one would expect based on the constant-property, fully developed results shown in Figure 2. In particular, for both Runs 618 and 635, the v^2–f model predicted the (absolute) wall temperatures to within approximately 1% of the experimental values near the location of maximum wall temperature (specifically, at $x/D = 25.3$). However, for Runs 618 and 635 the k–ω model underpredicted the wall temperatures at this location by 11% and 22%, respectively. For Run 445, both models underpredicted the wall temperatures, although the underprediction of the v^2–f model was only 1.5%, whereas the k–ω model underpredicted the wall temperature by 23% at $x/D = 25.3$.

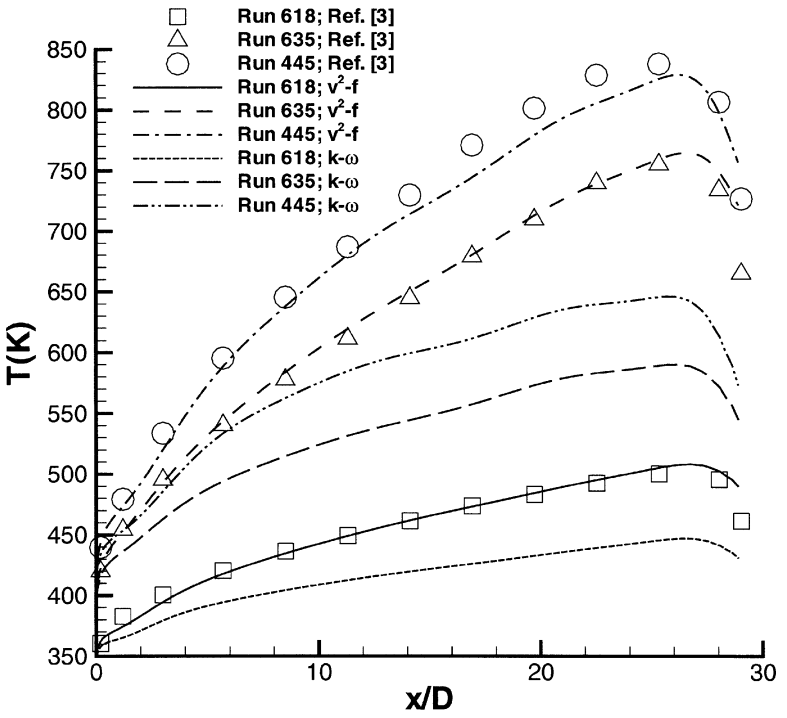

Figure 3. Comparison between local predicted wall temperatures and experimental data presented in [3].

In terms of modeling results presented by Mikielewicz et al. [5], the most effective model was the k–ε model of Launder and Sharma [6], which is a low-Reynolds-number model that utilizes damping functions in the near-wall region. That model overpredicted the maximum wall temperature by approximately 5% for Run 618, and 2.5% for Run 635. The maximum wall temperature was slightly underpredicted for Run 445. Relative to the Launder/Sharma model, the v^2–f model improved the predictions of the wall temperatures for Runs 618 and 635. For Run 445, the results from these two models were comparable. The least effective low-Reynolds-number k–ε model [27] examined by Mikielewicz et al. [5] provided results in terms of wall temperatures very similar to the low-Reynolds-number k–ω model. In fact, all of the low-Reynolds-number k–ε models except the Launder/Sharma model significantly underpredicted the local wall temperatures for each of the three levels of heating.

Mean velocity profiles at $x/D = 24.5$ are shown in Figures 4*a*–4*c* with the wall normal distance, y/R, plotted in log coordinates. Included in the figures are experimental results presented by Shehata and McEligot [3]. The velocity profiles have been rendered dimensionless with the local bulk velocity. The uncertainty in the experimental velocity data was reported in [5] to be in the range of 8–10%. For each level of heating, the figures reveal that in the near-wall region the velocities predicted by the v^2–f model are in good agreement with the experimental data, whereas the velocities are significantly overpredicted by the k–ω model. This observation is

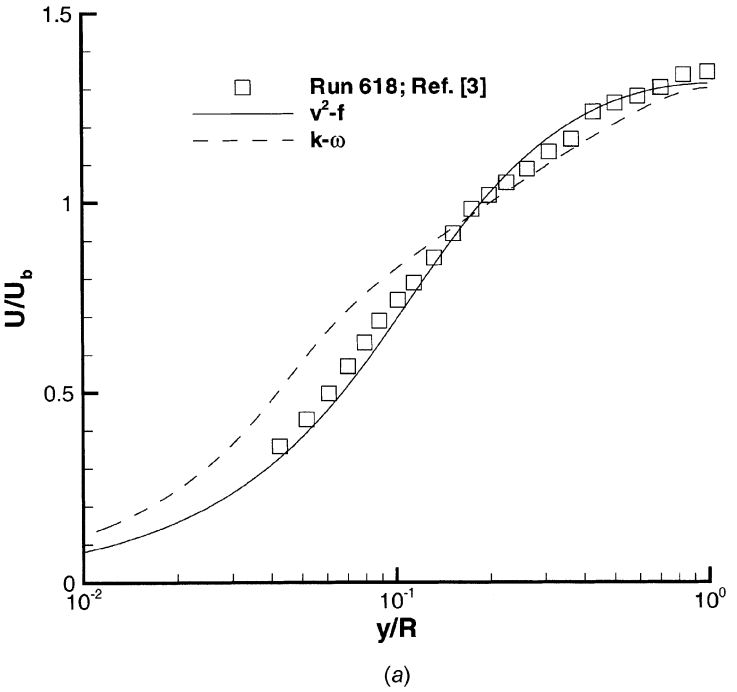

Figure 4. Comparison between predicted mean velocity profiles and experimental profiles at axial location $x/D = 24.5$: (*a*) Run 618; (*b*) Run 635; (*c*) Run 445.

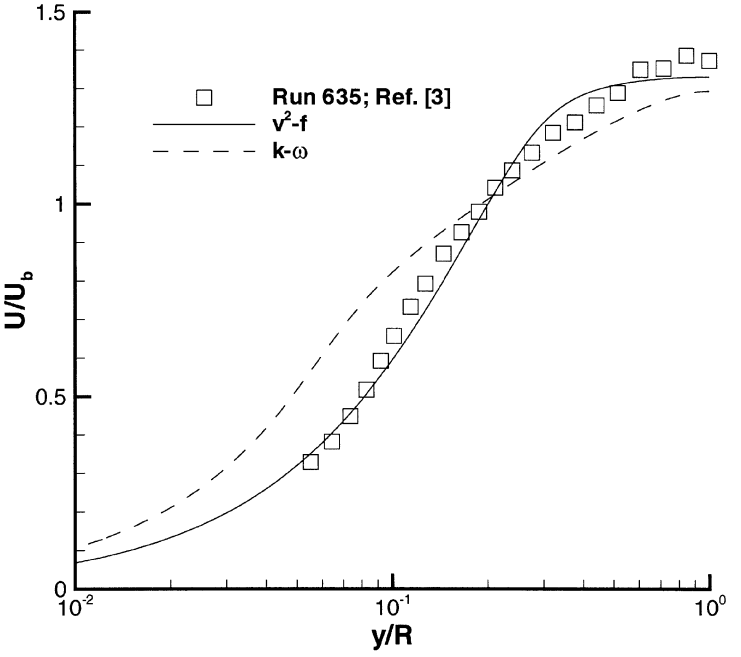

(*b*)

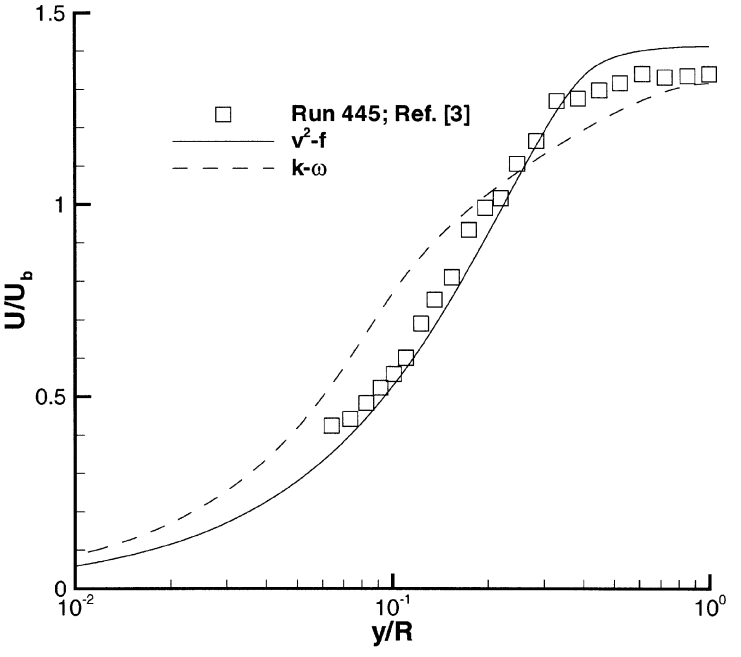

(*c*)

Figure 4. (Continued).

consistent with the results for the local wall temperatures shown in Figure 3. That is, the lower velocity in the near-wall region corresponds to lower heat transfer rates due to convection, resulting in higher wall temperatures.

Mean temperature profiles at station $x/D = 24.5$ are compared against the experimental data of Shehata and McEligot [3], in Figures 5*a*–5*c*, as a function of the wall normal distance. The temperatures have been nondimensionalized with their respective constant inlet temperatures. The uncertainty levels in the experimental data were previously reported at 1–2% of the local absolute temperature [5]. In general, the v^2–f model was able to predict quite accurately the radial temperature distributions for all three levels of heating. For Runs 618 and 635, the model slightly overpredicted the experimental values in the near-wall region, and slightly underpredicted the values beyond $y/R \approx 0.25$. For Runs 445, the dimensionless temperature profiles agree quite well with the experimental values over the entire region of the flow. However, the same cannot be said for the profiles obtained using the k–ω model. For each heating rate, the k–ω model considerably underpredicts the temperatures in the outer regions of the tube, and overpredicts the temperatures in the core region. This trend becomes more significant for the near-laminarizing case, Run 445. This is consistent with the constant-property results shown in Figure 2, in which the k–ω model was least accurate at the lower Reynolds numbers.

Shown in Figure 6 are the results of a grid resolution study for Run 618. Computed wall temperatures for both the v^2–f and k–ω models are presented as a

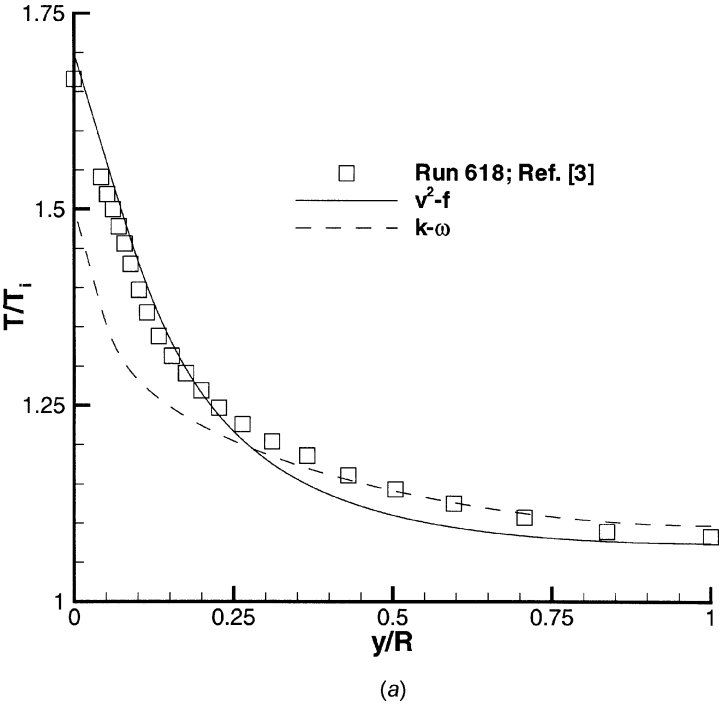

Figure 5. Comparison between predicted temperature profiles and experimental profiles at axial location $x/D = 24.5$: (*a*) Run 618; (*b*) Run 635; (*c*) Run 445.

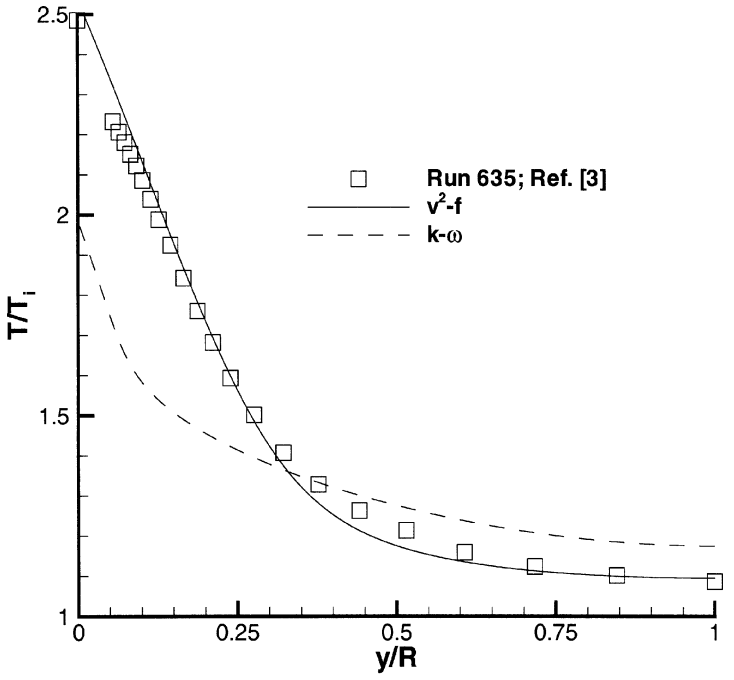

(*b*)

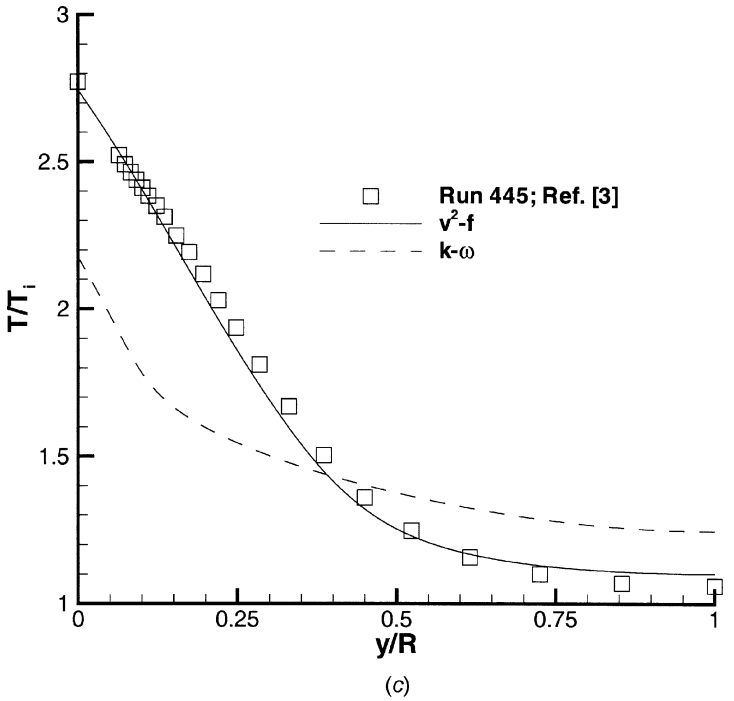

(*c*)

Figure 5. (Continued).

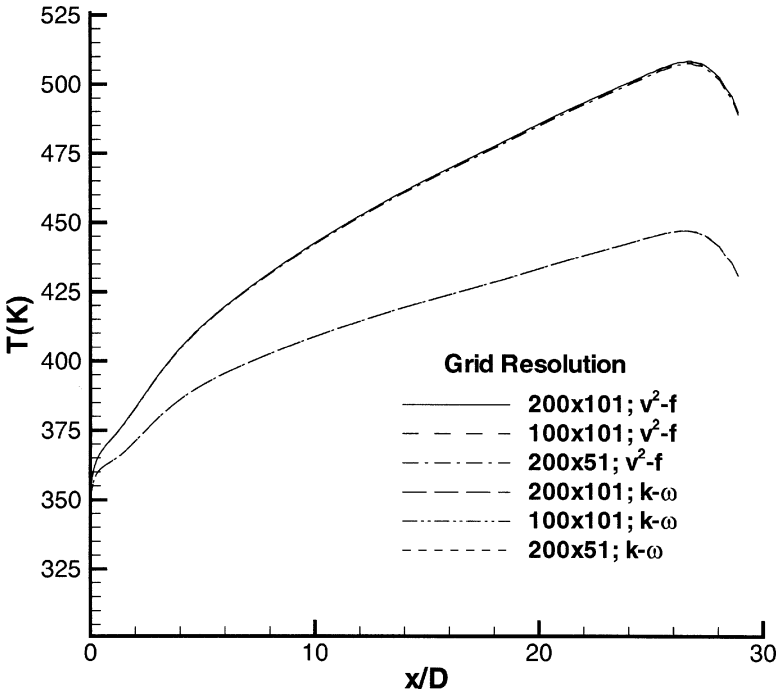

Figure 6. Results of a grid resolution study for Run 618 in which variation in local wall temperature is evaluated as a function of grid resolution and x/D.

function of x/D using grid resolutions of 200×101, 100×101, and 200×51 (streamwise by radial) points. (As previously discussed, results presented in Figures 3–5 were obtained using the 200×101 grid.) In each case, $y^+ < 0.5$ for the first node off the wall. The results clearly indicate that the solutions are grid independent on the 200×101 grid (the lines shown for each model are essentially coincident). In addition, mean flow profiles of both velocity and temperature computed using these three grids also showed no significant differences.

Finally, we show, in Figure 7, contours of constant (normalized) turbulence kinetic energy for Run 445 computed using the v^2–f turbulence model. Recall that $x/D = 0$ represents the beginning of the heated section. Consistent with our statements in the Introduction, these results clearly indicate the absence of a fully developed flow over the extent of the heated section. In addition, the results also reveal a strong decay in the levels of kinetic energy (nearly an order of magnitude) as the fluid properties vary, and the flow accelerates, along the heated section of the tube. This finding is consistent with the DNS results presented in [7]. Qualitatively similar results (although to a lesser extent) are found for Runs 618 and 635.

CONCLUSIONS

Both k–ω and v^2–f turbulence models were used to model an axisymmetric, strongly heated, low-Mach-number gas flowing upward within a vertical tube in which forced convection was dominant. However, the simpler case involving

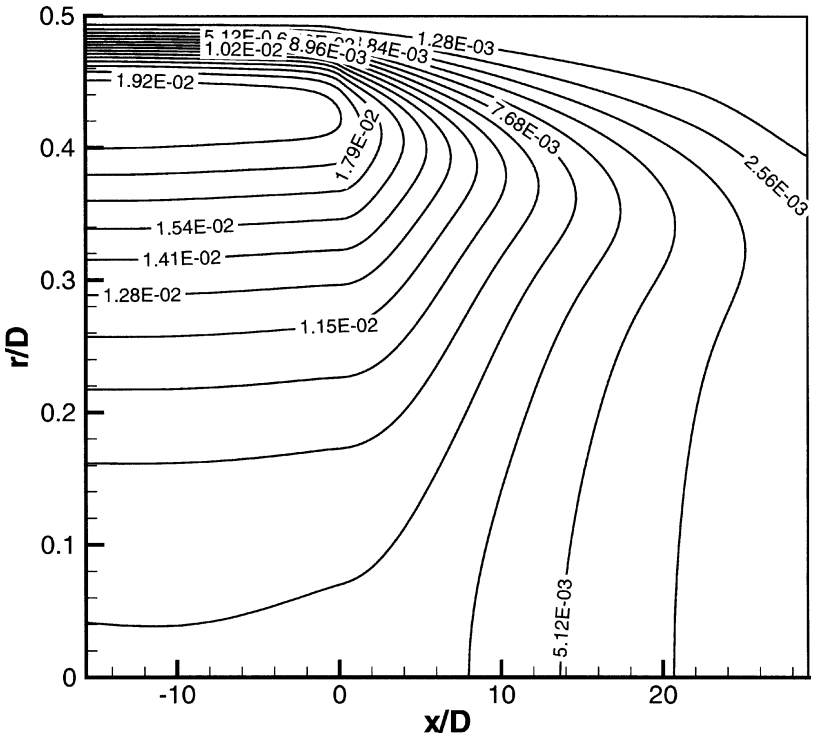

Figure 7. Contours of constant turbulence kinetic energy (normalized with respect to U_b^2) for Run 445 computed using the v^2–f model.

constant fluid property assumptions, which leads to a fully developed flow, was considered first. For the v^2–f model, results for these constant-property flow predictions were in close agreement with the Dittus-Boelter correlation [25], although some divergence was observed as the Reynolds number was increased. However, the results obtained using the k–ω model significantly overpredicted the Nusselt number over the range of Reynolds numbers of interest in this study.

Subsequent variable-property cases studied ranged from fully turbulent flow for Run 618 to nearly laminarized for Run 445. Over this range of flows, the v^2–f model was able to predict the experimental data for wall temperatures to within acceptable engineering accuracy. The model provided improved results over the series of low-Reynolds-number k–ε models that were previously applied to this flow by Mikielewicz et al. [5]. Conversely, the k–ω model performed in a manner consistent with the bulk of the two-equation models evaluated in the Mikielewicz et al. study, significantly overpredicting wall heat transfer rates.

REFERENCES

1. K. R. Perkins, Turbulence Structure in Gas Flows Laminarizing by Heating, Ph.D. thesis, University of Arizona, Tucson, AZ, 1975.
2. A. M. Shehata, Mean Turbulence Structure in Strongly Heated Air Flows, Ph.D. dissertation, University of Arizona, Tucson, AZ, 1984.

3. A. M. Shehata and D. M. McEligot, Turbulence Structure in the Viscous Layer of Strongly Heated Gas Flows, Tech. Rep. INEL-95/0223, Idaho National Engineering Laboratory, Idaho Falls, IO, 1995.
4. A. M. Shehata and D. M. McEligot, Mean Turbulence Structure in the Viscous Layer of Strongly-Heated Internal Gas Flows: Measurements, *Int. J. Heat Mass Transfer*, vol. 41, pp. 4297–4313, 1998.
5. D. P. Mikielewicz, A. M. Shehata, J. D. Jackson, and D. M. McEligot, Temperature, Velocity and Mean Turbulence Structure in Strongly Heated Gas Flows: Comparison of Numerical Predictions with Data, *Int. J. Heat Mass Transfer*, vol. 45, pp. 4333–4352, 2002.
6. B. Launder and B. Sharma, Application of Energy-Dissipation Model of Turbulence to the Calculation of Flow near a Spinning Disk, *Lett. Heat Transfer*, vol. 1, pp. 131–138, 1974.
7. S. Satake, T. Kunugi, A. M. Shehata, and D. M. McEligot, Direct Numerical Simulation for Laminarization of Turbulent Forced Gas Flows in Circular Tubes with Strong Heating, *Int. J. Heat Fluid Flow*, vol. 21, pp. 526–534, 2000.
8. K. Ezato, A. M. Shehata, T. Kunugi, and D. M. McEligot, Numerical Prediction of Transitional Features of Turbulent Forced Gas Flows in Circular Tubes with Strong Heating, *J. Heat Transfer*, vol. 121, pp. 546–555, 1999.
9. K. Abe, T. Kondoh, and Y. Nagano, A New Turbulence Model for Predicting Fluid Flow and Heat Transfer in Separating and Reattaching Flows—I. Flow Field Calculations, *Int. J. Heat Mass Transfer*, vol. 37, pp. 139–151, 1994.
10. M. Nishimura, S. Fujii, A. M. Shehata, T. Kunugi, and D. M. McEligot, Prediction of Forced Gas Flows in Circular Tubes at High Heat Fluxes Accompanied by Laminarization, *J. Nuclear Sci. Technol.*, vol. 37, pp. 581–594, 2000.
11. K. Takase, Numerical Prediction of Augmented Turbulent Heat Transfer in an Annular Fuel Channel with Repeated Two-Dimensional Square Ribs, *Nuclear Eng. Design*, vol. 165, pp. 225–237, 1996.
12. K. Takase, Three-Dimensional Numerical Simulations of Heat Transfer in an Annular Fuel Channel with Periodic Spacer Ribs under a Fully Developed Turbulent Flow, *Nuclear Technol.*, vol. 118, pp. 175–185, 1996.
13. K. Takase, Three-Dimensional Numerical Simulations of Heat Transfer in an Annular Fuel Channel with Epriodic Spacer Ribs under a Fully Developed Turbulent Flow, *Nuclear Technol.*, vol. 118, pp. 175–185, 1997.
14. S. Fujii, N. Akino, M. Hishida, H. Kawamura, and K. Sanokawa, Experimental and Theoretical Investigations on Heat Transfer of Strongly Heated Turbulent Gas Flow in an Annular Duct, *JSME Int. J., Ser. II*, vol. 34, pp. 348–354, 1991.
15. D. W. Wilcox, *Turbulence Modeling for CFD*, 2d ed., DCW Industries, La Cañada, CA, 1998.
16. P. A. Durbin, Near-Wall Turbulence Closure Modeling Without Damping Functions, *Theoret. Comput. Fluid Dynam.*, vol. 3, pp. 1–13, 1991.
17. M. Behnia, S. Parneix, Y. Shabany, and P. A. Durbin, Numerical Study of Turbulent Heat Transfer in Confined and Unconfined Impinging Jets, *Int. J. Heat Fluid Flow*, vol. 20, pp. 1–9, 1999.
18. P. A. Durbin, Application of a Near-Wall Turbulence Model to Boundary Layers and Heat Transfer, *Int. J. Heat Fluid Flow*, vol. 14, pp. 316–323, 1993.
19. R. Manceau, J. R. Carlson, and T. B. Gatski, A Rescaled Elliptic Relaxation Approach: Neutralizing the Effect on the Log Layer, *Phys. Fluids*, vol. 14, pp. 3868–3878, 2002.
20. F. S. Lien and P. A. Durbin, Non-linear k–ε–v^2 Modeling with Application to High Lift, Center for Turbulence Research, Proceedings of the Summer Program, 1996.

21. D. Cokljat, S. E. Kim, G. Iaccarino, and P. A. Durbin, A Comparative Assessment of the V2F Model for Recirculating Flows, AIAA-2003-0765, 41st Aerospace Sciences Meeting and Exhibit, Reno, NV, January 6–9, 2003.
22. S. Patankar, *Numerical Heat Transfer and Fluid Flow*, Hemisphere, New York, 1980.
23. J. H. Ferziger and M. Peric, *Computational Methods for Fluid Dynamics*, Springer Verlag, New York, 1996.
24. B. A. Kader and A. M. Yaglom, Heat and Mass Transfer Laws for Fully Turbulent Wall Flows, *Int. J. Heat Mass Transfer*, vol. 15, pp. 2239–2351, 1972.
25. F. W. Dittus and L. M. K. Boelter, Heat Transfer in Automobile Radiators of the Tubular Type, *Univ. Calif. Publ. Eng.*, vol. 2, pp. 443–461, 1930; reprinted in *Int. Commun. Heat Mass Transfer*, vol. 12, pp. 3–22, 1985.
26. D. M. McEligot, L. W. Ormand, and H. C. Perkins, Internal Low Reynolds Number Turbulent and Transitional Gas Flow with Heat Transfer, *J. Heat Transfer*, vol. 88, pp. 239–245, 1966.
27. T. H. Shih and A. T. Hsu, An Improved k–ε Model for Near-Wall Turbulence, AIAA Paper 91-0611, 1991.